Global Biogeochemical Cycles

RESEARCH ARTICLE
10.1029/2025GB008804

Global Natural Soil N_2O Emissions: An Analysis With a Global Biogeochemistry Model From 1990 to 2023

Ye Yuan[1] and **Qianlai Zhuang**[1,2]

[1]Department of Earth, Atmospheric, and Planetary Science, Purdue University, West Lafayette, IN, USA, [2]Department of Agronomy, Purdue University, West Lafayette, IN, USA

Key Points:

- Global undisturbed natural soil N_2O emissions rose steadily (1990–2023), with tropics contributing ~70% of the total flux
- Using observed land cover (European Space Agency Climate Change Initiative) leads to 30% lower N_2O estimates compared with potential vegetation due to forest fragmentation
- Majority of N_2O emissions come from background processes, then N fixation, N deposition, and rock weathering

Supporting Information:

Supporting Information may be found in the online version of this article.

Correspondence to:

Q. Zhuang,
qzhuang@purdue.edu

Citation:

Yuan, Y., & Zhuang, Q. (2026). Global natural soil N_2O emissions: An analysis with a global biogeochemistry model from 1990 to 2023. *Global Biogeochemical Cycles*, *40*, e2025GB008804. https://doi.org/10.1029/2025GB008804

Received 21 AUG 2025
Accepted 25 MAR 2026

Abstract Atmospheric N_2O, the dominant ozone-depleting substance and a potent greenhouse gas, has risen notably over recent decades. Using a process-based model, we simulated the sensitivity of N_2O emissions from undisturbed natural soils to the representation of historical land-cover change from 1990 to 2023 by factoring the effects of atmospheric nitrogen deposition, biological nitrogen fixation, rock weathering, and soil uptake. Simulations based on the potential vegetation distribution data show average emissions of 6.24 ± 0.72 Tg N yr^{-1} with a significant upward trend (+0.021 Tg N yr^{-1}) from 1990 to 2023, while European Space Agency Climate Change Initiative land cover estimates were 30% lower, underscoring the sensitivity of N_2O estimates to land-cover representation. Most emissions stem from background processes (69.8% ± 4.5%), followed by nitrogen fixation (16.3% ± 2.6%), atmospheric deposition (9.2% ± 1.3%), and rock weathering (4.7% ± 1.1%). The accelerating trend of N_2O emissions under changing climate conditions and key uncertainties are tied to used land-cover data sets, limited observation data, and unresolved hydrological extremes.

Plain Language Summary Nitrous oxide (N_2O) is a powerful greenhouse gas that also depletes the ozone layer. Natural ecosystems, such as forests, grasslands, and wetlands, play an important role in releasing N_2O into the atmosphere. In this study, we used a process-based ecosystem model and high-resolution land cover data from satellites to estimate how much N_2O has been emitted globally by natural ecosystems from 1990 to 2023. We found that tropical regions contributed most of the emissions and that human-driven land-cover changes, such as deforestation, have significantly altered the natural N_2O budget. This work helps improve our understanding of how natural terrestrial ecosystems contribute to climate change and supports future efforts to monitor and reduce greenhouse gas emissions.

1. Introduction

Nitrous oxide (N_2O) is the leading ozone-depleting substance and a potent long-lived greenhouse gas. Its atmospheric concentrations have risen from 270 ppb in 1750 to 336 ppb in 2023, with an accelerated increase since 1980 (Butterbach-Bahl et al., 2013; Tian et al., 2024).

Globally, the largest sources of N_2O emissions originate from natural soil processes (Tian et al., 2024). To estimate large-scale gaseous nitrogen (N) losses from terrestrial ecosystems, researchers have developed a range of methodologies, broadly categorized into bottom-up and top-down approaches. Bottom-up methods encompass inventory-based assessments, statistical extrapolations of field measurements, mass balance techniques, and process-based modeling (Harris et al., 2022; Kroeze et al., 1999; Tian et al., 2024), while top-down approaches use atmospheric inversion techniques to infer emissions based on observed atmospheric concentrations (Thompson et al., 2019). Among bottom-up approaches, process-based modeling stands out for its ability to explicitly simulate the underlying biogeochemical processes that control N_2O emissions while integrating diverse environmental and anthropogenic drivers. Their ability to resolve spatial and temporal emission patterns makes them especially useful in regions with high nitrogen inputs (Thompson et al., 2019; Tian et al., 2024).

Many current process-based land models primarily represent internal nitrogen cycling, and typically include only biological nitrogen fixation (BNF) and atmospheric nitrogen deposition as external nitrogen inputs, with deposition prescribed from atmospheric chemistry model products (Stocker et al., 2016; Vitousek et al., 2013). Models such as CLM4.5, CLM5, JSBACH, JULES-ES, LPJ-GUESS, CLASSIC, ELM, ORCHIDEE, and LPX-Bern typically rely on simplified, empirical representations of BNF and deposition (Asaadi & Arora, 2021; Davies-Barnard et al., 2020; Ghimire et al., 2016; Goll et al., 2017; Lawrence et al., 2019; Ma et al., 2022; Mathison

et al., 2023; Tian et al., 2024; Vuichard et al., 2019; Zhu et al., 2019), while neglecting other potentially important sources such as nitrogen released through rock weathering. Recent studies have identified rock weathering as a significant and widespread source of reactive nitrogen that can contribute to N_2O emissions (Houlton et al., 2018; Morford et al., 2016; Wan et al., 2021; Wooliver et al., 2019). Moreover, nitrogen losses such as ammonia (NH_3) volatilization are often omitted, and mechanistic representations of both symbiotic and free-living nitrogen fixation are generally lacking (Yuan, Zhuang, Zhao, & Liu, 2025). These limitations underscore the need for more comprehensive modeling frameworks that integrate multiple nitrogen sources and loss pathways to improve the understanding of terrestrial nitrogen cycling and its contribution to N_2O emissions. The spatiotemporal variability of nitrogen deposition further complicates accurate quantification of soil N_2O fluxes, contributing to significant uncertainty in nitrogen–climate interactions within the Earth system. Some bottom-up N_2O studies have used potential vegetation or pre-industrial land-cover maps as proxies for actual land cover, potentially overlooking the effects of contemporary land use (Tian et al., 2024). Such frameworks treat potential vegetation as a static baseline against which historical land-use and land-cover change (LUC) effects are quantified, introducing uncertainty in the representation of background N_2O emissions. While large-scale initiatives such as the Global N_2O Model Intercomparison Project (NMIP) employ dynamic land-cover data to account for LUC, the specific sensitivity of natural soil N_2O emissions to the static versus dynamic representation of natural vegetation extent has not been systematically isolated.

Land-cover change exerts substantial biogeochemical and biophysical impacts on climate by altering greenhouse gas emissions and surface energy balance, through shifts in albedo, evapotranspiration, and surface roughness (Liu et al., 2017; Pielke, 2005). These changes have been shown to significantly affect simulations of energy, water, and carbon fluxes in global land surface models (Harper et al., 2023). In particular, deforestation is responsible for an estimated 53%–58% of the difference between current and potential biomass stocks (Erb et al., 2018), which has substantial implications for N_2O emissions from natural terrestrial ecosystems. The exclusion of actual land cover dynamics in modeling frameworks may therefore lead to significant biases in the simulation of nitrogen cycling and associated greenhouse gas fluxes.

In this study, we enhanced the Terrestrial Ecosystem Model (TEM) by integrating a more comprehensive nitrogen cycle framework that includes additional nitrogen input and output processes and integrating land cover data derived from the European Space Agency Climate Change Initiative (ESA-CCI; Copernicus Climate Change Service, 2019) to address the gap by providing a targeted, diagnostic analysis of how the assumption of a static potential vegetation baseline affects simulated natural soil N_2O emissions, independent of managed lands, fertilizer application, or other anthropogenic inputs. The updated TEM was calibrated, validated, and applied to quantify N_2O emissions from natural terrestrial ecosystems globally over the period 1990–2023.

2. Method

2.1. Description of TEM

The TEM is a global biogeochemical model that simulates water, carbon (C), and nitrogen (N) cycling in terrestrial ecosystems (McGuire et al., 1997; Melillo et al., 1993; Yuan, Zhuang, Zhao, & Liu, 2025; Yuan, Zhuang, Zhao, & Shurpali, 2025; Zhuang et al., 2002, 2003). The nitrogen dynamics module builds on earlier work (McGuire et al., 1997; Yuan, Zhuang, Zhao, & Shurpali, 2025, Yuan, Zhuang, Zhao, & Shurpali, 2025) and incorporates key processes including nitrogen inputs from plant litter and atmospheric deposition, biological N fixation, plant uptake, net mineralization, and nitrogen losses. The module also represents the influence of soil physical conditions on nitrification, denitrification, and N_2O fluxes. TEM simulates both N_2O production within soil and net N_2O emission to the atmosphere. Net N_2O emission is calculated as the difference between N_2O production and soil N_2O uptake, with gas transport represented using Fick's law (Equations S1–S12, Yuan, Zhuang, Zhao, & Shurpali, 2025). These processes follow the stoichiometric principles of soil C-N interactions. In this study, we revise the N cycling algorithms in TEM by adding nitrogen inputs from bedrock weathering and outputs via NH_3 volatilization (Figure 1). Inorganic N from weathering is derived from Houlton et al. (2018) and Wan et al. (2021), while NH_3 volatilization is simulated using process-based algorithms adopted from Montes et al. (2009) and Zhao and Zhuang (2024), which were developed and evaluated against observational data sets in their respective studies.

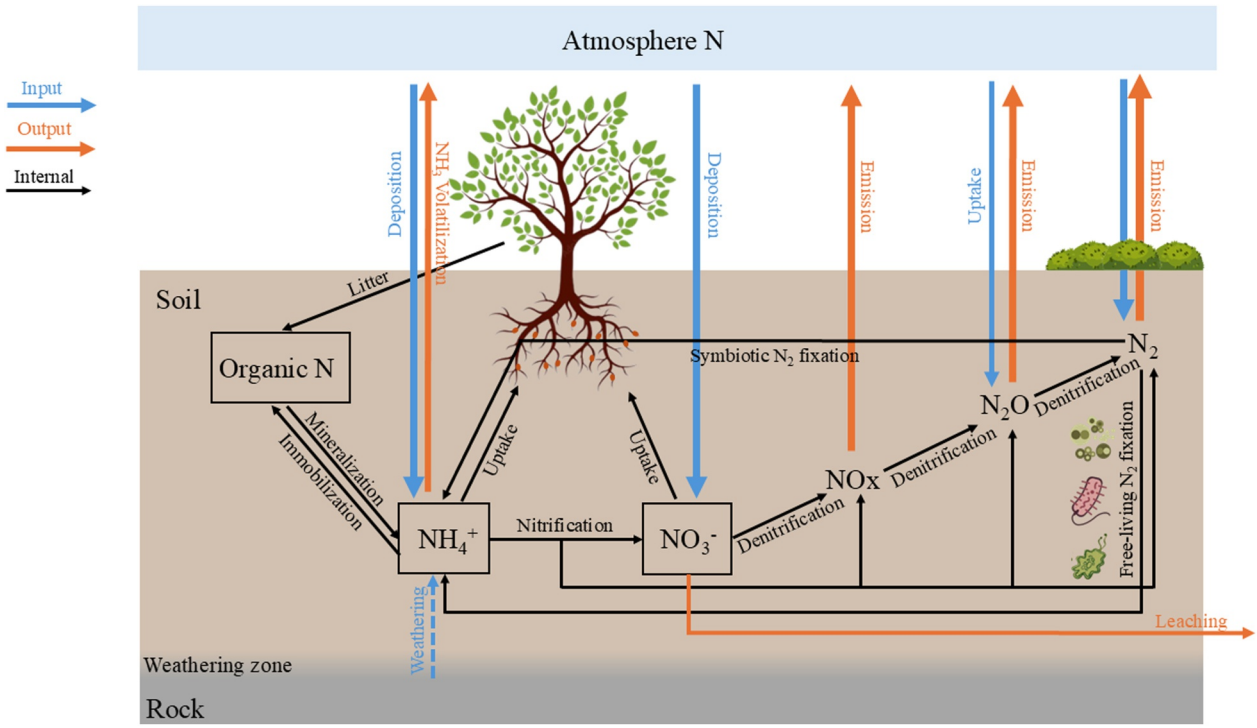

Figure 1. Structure of the nitrogen (N) cycle in Terrestrial Ecosystem Model (TEM), including three main components: external N inputs, internal cycling, and N outputs. Blue arrows indicate N input pathways, including atmospheric deposition, nitrogen release from rock weathering, biological nitrogen fixation, and atmospheric gas uptake. Orange arrows represent N output pathways, including leaching and gaseous losses (e.g., NH_3, NO_x, N_2O, and N_2). Black arrows illustrate internal nitrogen cycling within TEM, including litterfall, mineralization, immobilization, plant uptake, nitrification, and denitrification. Nitrogen leaching is represented primarily as nitrate loss because NO_3^- is highly mobile in soil water. Immobilization is represented mainly as microbial uptake of NH_4^+, reflecting the lower energetic cost of ammonium assimilation compared with nitrate reduction.

2.2. Model Calibration, Validation, and Uncertainties

Observational data for model calibration and evaluation were compiled from peer-reviewed literature using the keywords "N_2O" or "nitrous oxide." Data were obtained either directly from the authors or digitized from published figures. Only observations spanning ≥4 months were included, and screened for outliers using Q–Q plots and Z-score filtering. The final data set comprised 1,062 observations from 65 sites across diverse ecosystems, including 4 Xeric Shrubland/Woodland, 3 Mediterranean Shrubland, 7 Wet Tundra, 5 Alpine/Dry Tundra, 8 Grassland, 7 Boreal Forest, 3 Temperate Evergreen Forest, 8 Temperate Coniferous Forest, 9 Temperate Deciduous Forest, and 11 Tropical Forest sites (Figure S1 and Table S1 in Supporting Information S1).

Model calibration and validation were performed for each plant functional type (PFT) using Bayesian optimization with 5-fold stratified cross-validation to ensure balanced site representation. Calibrations were aligned exactly with the measurement periods of each site to ensure temporal consistency. N_2O emissions were aggregated to monthly rates for comparison because the model was run at a monthly time step, which corresponds to the monthly resolution of the primary input data. In addition, our study focuses on long-term trends and mean annual balances, for which a monthly time step provides an appropriate balance between computational efficiency and capturing the essential system dynamics. This temporal aggregation also helps reduce noise that may arise from daily or hourly variability.

Bayesian optimization was implemented via the Python package *scikit*, and the parameter set with the lowest RMSE across folds was selected as the best-performing set to drive TEM simulations (Table S4 in Supporting Information S1). Simulated cumulative N_2O emissions using the best performing parameter set closely matched observations, capturing site-level annual cumulative N_2O emissions across a range of biomes (Figure S2 in Supporting Information S1). This validation confirms the model's utility for estimating large-scale, long-term fluxes. However, the comparison at the annual timescale indicates that the model's ability to simulate high-frequency (e.g., daily or monthly) temporal variability is limited, consistent with the model's design and resolution.

To assess uncertainty, we conducted ensemble simulations using all five parameter sets, providing a robust estimate of parameter-driven variability.

2.3. Regional Extrapolation

To generate spatially and temporally explicit global N_2O emission estimates, we ran TEM at a 0.5° × 0.5° resolution using land cover, soil, and climate data sets from various sources (Table S5 in Supporting Information S1). Monthly climate forcing (1990–2023) was obtained from ERA5 (Hersbach et al., 2023), and atmospheric CO_2 concentrations from the NOAA Global Monitoring Laboratory (NOAA Global Monitoring Laboratory, 2025). Soil bulk density and pH data were sourced from the Global Soil Bulk Density Map and Global Database of Soil Properties (Carter & Scholes, 2000; Global Soil Data Task, 2000). Nitrogen deposition (NH_x and NOγ) was derived from ACCMIP multi-model data sets (Lamarque et al., 2013) for 1980, 2000, and 2030, with linear interpolation applied between years. The sensitivity of our results to this interpolation was tested against time-series nitrogen deposition data from Tian et al. (2022), as discussed in Section 3.6. Bedrock weathering fluxes were based on Houlton et al. (2018), assuming that all nitrogen enters the soil as NH_4^+ (Houlton et al., 2018; Wan et al., 2021). These data were resampled and formatted for TEM, including model modifications to accommodate NH_x, NOγ, and rock weathering N inputs. We spun up TEM using fixed climate forcing to reduce sensitivity to initial conditions and allow ecosystem pools to approach equilibrium for subsequent transient simulations. The model was initialized using a cyclic forcing of the first 30-year climate sequence, repeated for 5 cycles to reach a total of 150 years. This length is consistent with our previous studies (Qu et al., 2018). During spin-up, the equilibrium of the water, carbon, and nitrogen cycles was evaluated using predefined absolute tolerance thresholds.

2.4. Land Use and Land Cover Change

In addition to using the potential vegetation map (PVM) from Melillo et al. (1993), we incorporated land cover information from the ESA-CCI data set at 300 m resolution, spanning 1992 to 2022, to assess the impact of historical land use and land cover change on natural ecosystem N_2O emissions. Annual ESA land cover maps at 300 m resolution were aggregated by applying 0.5° × 0.5° resolution mask and summarizing land cover types and pixel numbers within each grid cell. Referring to the cross-walking table provided by Harper et al. (2023), ESA land cover classes were converted into fractional PFTs and subsequently mapped to the TEM-specific PFT categories (Table S2 and S3 in Supporting Information S1), allowing up to six TEM-PFTs per 0.5° × 0.5° grid cell. Each land cover configuration was simulated individually. Total N_2O emissions were computed by summing the emissions from each PFT multiplied by their area in each grid. This approach allowed for high-resolution representation of land cover dynamics while maintaining computational efficiency.

2.5. Statistic Analysis

Statistical analyses were conducted in R 4.3.3 (R Core Team, 2024). Trends in global N_2O fluxes were evaluated using the Mann-Kendall test and Sen's slope via the "trend" package. Differences across PFTs were assessed with one-way ANOVA and post hoc Tukey's HSD tests using the "stats" package.

3. Results

3.1. Global Estimation of Terrestrial Natural Ecosystem N_2O Emissions

Global net N_2O emissions averaged 6.24 ± 0.72 Tg N yr^{-1} from 1990 to 2023, with annual values ranging from 5.84 Tg N yr^{-1} in 1990 to a peak of 6.92 Tg N yr^{-1} in 2009. Emissions exhibited pronounced interannual variability, with peaks in 2009 and 2022 (6.92 and 6.82 Tg N yr^{-1}, respectively) and a trough in 1995 (5.88 Tg N yr^{-1}). N_2O production followed a similar trajectory but remained consistently higher, averaging 6.57 ± 0.45 Tg N yr^{-1}, reflecting a persistent production-emission gap (Figure 2). Model uncertainty was substantial. For the potential vegetation simulations, the lower bounds ranged from 1.85 to 2.33 Tg N yr^{-1}, while for the ESA-CCI based simulations they ranged from 2.70 to 3.25 Tg N yr^{-1}, likely reflecting limitations in parameterization and observational constraints. The upper bounds were 5.92–7.08 Tg N yr^{-1} for the potential vegetation case and 4.17–5.15 Tg N yr^{-1} for the ESA-based case, both closely aligned with the estimates from the best-performing parameter set. Emission estimates based on the ESA-CCI land-cover data set were systematically lower than those derived from the PVM, averaging 4.14–4.70 Tg N yr^{-1}. On average, using time-series land

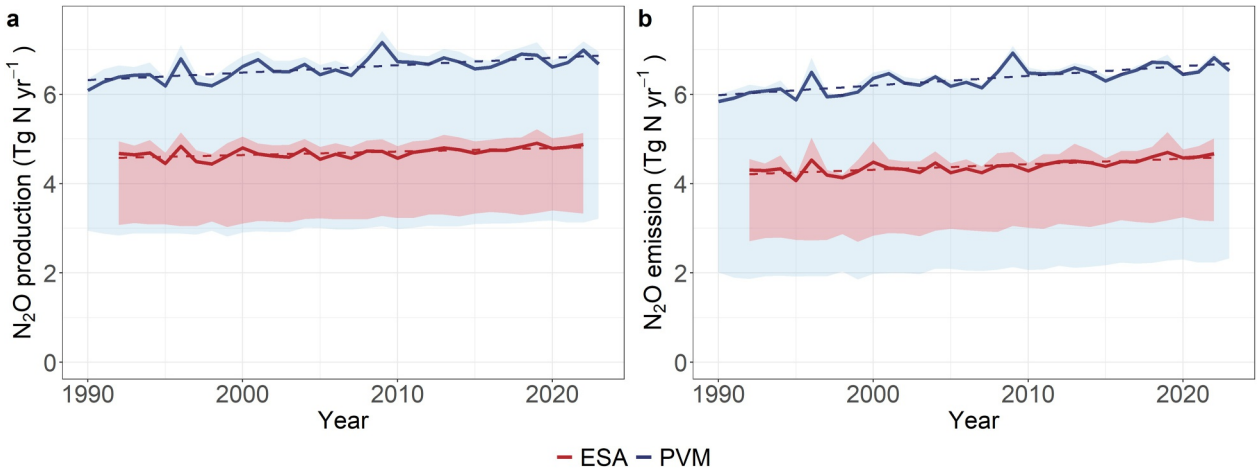

Figure 2. Global N_2O production (a) and N_2O emissions (b) under different land cover representations. "ESA" denotes estimates derived from the European Space Agency Climate Change Initiative land cover data set, while "PVM" represents estimates based on the potential vegetation map. The shaded blue and red areas indicate the range of model uncertainties resulting from parameter variability, derived from an ensemble of five parameter sets obtained through stratified cross-validation.

cover, the ESA-based estimates accounted for 69.15% ± 1.54% of net emissions and 70.95% ± 1.47% of N_2O production relative to PVM-based estimates, reflects historical conversion yields estimates of N_2O emissions from remaining natural soils that are 30% lower than estimates based on potential vegetation, underscoring the strong sensitivity of modeled global N_2O fluxes to land-cover representation. Mann-Kendall test revealed significant upward trends in N_2O emissions and production across all data sets. On average, N_2O emissions during 2019–2023 were 0.6 Tg N yr^{-1} (approximately 10%) higher than those during 1990–1994. Modeled N_2O production showed a strong increasing trend ($p < 0.001$; Sen's slope = 0.016 Tg N yr^{-1}, 95% CI: 0.008–0.022), while net emissions exhibited an even steeper trend ($p < 0.001$; slope = 0.021 Tg N yr^{-1}, 95% CI: 0.014–0.027). Although trends from the ESA-CCI based estimates were less pronounced due to a shorter time series ($n = 31$), they remained statistically significant for both production ($p < 0.05$; slope = 0.008 Tg N yr^{-1}, 95% CI: 0.004–0.01) and net emissions ($p < 0.001$; slope = 0.014 Tg N yr^{-1}, 95% CI: 0.009–0.018). These consistently positive and statistically robust trends across data sets confirm that global N_2O emissions have accelerated significantly from 1990 to 2023, with variation in magnitude driven primarily by land-cover inputs.

3.2. Spatial Distribution

Spatially, tropical regions exhibited the highest N_2O production and emissions (orange areas in panels a–d, Figure 3), whereas the northern high latitudes and global drylands showed low emissions and functioned as net N_2O sinks (blue areas in panels c–d, Figure 3). The latitudinal distribution clearly identified the tropics (0°–23.5°) as dominant hotspots, accounting for approximately 70% of global N_2O emissions. Between 1990–1994 and 2019–2023, both N_2O production and emissions increased globally, with the most significant growth observed in tropical and subtropical zones. However, regional variability is evident: while much of the tropics experienced rising emissions, certain areas, such as central South America and central Africa, exhibited localized declines, potentially linked to climate variability or shifts in nitrogen inputs. In contrast, emissions in temperate regions showed moderate increases, while boreal emissions remained relatively stable (Figure 3).

3.3. Production and Emission Variations Across Different Plant Functional Types

N_2O emissions varied significantly among PFTs ($p < 0.001$), with tropical forests exhibiting the highest mean emissions (0.114 ± 0.006 g N m^{-2} yr^{-1}), followed by temperate deciduous forests (0.038 ± 0.003 g N m^{-2} yr^{-1}) and grasslands (0.035 ± 0.006 g N m^{-2} yr^{-1}) (Figure S3 in Supporting Information S1). No significant differences were found between Mediterranean shrublands and alpine tundra ($p = 0.64$), or between temperate evergreen forests and shrublands ($p = 0.89$), suggesting similar underlying emission drivers in these ecosystems. The lowest emissions occurred in wet tundra and temperate evergreen forests, both below 0.01 g N m^{-2} yr^{-1}.

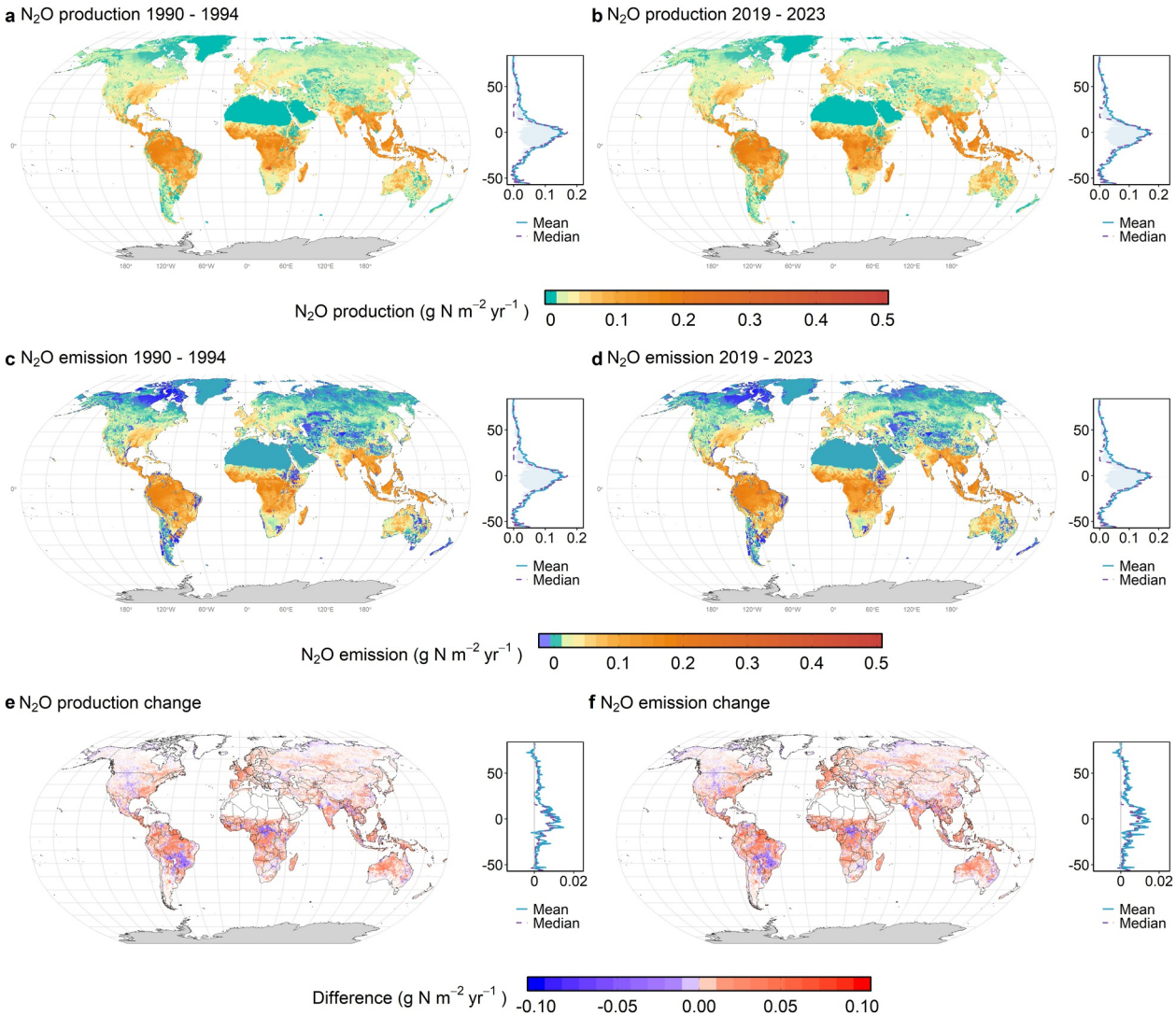

Figure 3. Spatial patterns and latitudinal distributions of N_2O production and emissions based on the potential vegetation map. Panels (a) and (b) show the spatial distribution and latitudinal profile of N_2O production, averaged over two 5-year periods: 1990–1994 and 2019–2023, respectively. Panels (c) and (d) present N_2O emissions for the same time periods. Panels (e) and (f) show the changes in average N_2O production and emissions between 1990–1994 and 2019–2023, respectively (2019–2023 minus 1990–1994).

N_2O production also differed significantly among PFTs ($p < 0.001$). Tropical forest again showed the highest production rates (0.115 ± 0.005 g N m^{-2} yr^{-1}), approximately 9.5 times greater than in alpine tundra (0.011 ± 0.0003 g N m^{-2} yr^{-1}). Temperate deciduous forests (0.042 ± 0.002 g N m^{-2} yr^{-1}) and grassland (0.037 ± 0.002 g N m^{-2} yr^{-1}) followed. Boreal forests and temperate conifer forests had comparable production rates (~0.018 g N m^{-2} yr^{-1}; $p > 0.05$), while Mediterranean shrublands and temperate evergreen forest were slightly lower (0.017–0.018 g N m^{-2} yr^{-1}). Wet tundra and alpine tundra had the lowest N_2O production, though wet tundra emissions were marginally higher than alpine tundra ($p < 0.05$). Interquartile range (IQR) values (e.g., tropical forest: 0.006; alpine tundra: 0.0003) indicate a greater variability in high-emission PFTs, suggesting stronger environmental sensitivity in tropical regions.

3.4. Seasonal Variability in N_2O Productions and Emissions

Figure S4 in Supporting Information S1 highlights strong seasonal contrasts in N_2O fluxes between tropical and temperate regions. Tropical ecosystems emitted more N_2O annually (0.008 ± 0.0006 g N m^{-2} yr^{-1}) than temperate ecosystems (0.002 ± 0.001 g N m^{-2} yr^{-1}), with emissions peaking in October and showing low

seasonal variation (CV = 7%). In contrast, temperate regions displayed pronounced seasonality, with summer peaks (July: 0.004 g N m^{-2} yr^{-1} in the Northern Hemisphere; January: 0.005 g N m^{-2} yr^{-1} in the Southern Hemisphere) and winter lows (December: 0.0004 g N m^{-2} yr^{-1} in the Northern Hemisphere; July: 0.001 g N m^{-2} yr^{-1} in the Southern Hemisphere). This resulted in seasonal amplitudes of nearly 9.7-fold in the Northern Hemisphere and 4.7-fold in the Southern Hemisphere, with high variability (CV = 83% and 37%, respectively). The tropical-to-temperate emission ratio ranged from 1.92 during summer to 19.37 in winter, underscoring the disproportionate contribution of tropical systems to the global N_2O budget, particularly outside the growing season.

3.5. The Effects of Actual Land Use and Land Cover Change

The natural area represented in the ESA-CCI land cover data set covers 79.33 ± 0.14% of that in the potential vegetation map (PVM; 133,561,319 km^2). This discrepancy likely accounts for the lower N_2O estimates in ESA-based simulations, yielding only 69.15 ± 1.54% of net emissions and 70.95 ± 1.47% of production compared to PVM-based results. Among PFTs, only grassland and alpine tundra show greater spatial extent in ESA-CCI relative to the TEM PVM; all other PFTs exhibit reduced coverage. The most significant decline is observed in tropical forests, the PFT with the highest N_2O emission rates that occupies just 44.5 ± 0.54% of their potential extent in the ESA-CCI data set. This substantial reduction largely explains the lower N_2O fluxes in ESA-based simulations. This finding aligns with Harper et al. (2023), who demonstrated that incorporating ESA-CCI-based PFT maps into the ORCHIDEE model significantly altered energy, water, and carbon fluxes, particularly in areas where woody vegetation was replaced by grasslands or bare soil, patterns that mirror our findings for nitrogen fluxes. Notably, N_2O emission hotspots in tropical regions frequently coincide with zones of rapid land-use change and agricultural expansion. Their persistence and spatial expansion over recent decades underscore the growing influence of tropical ecosystems on the global N_2O budget and highlight their vulnerability to anthropogenic pressures.

In addition to tropical forests, temperate deciduous forest (23.93% ± 0.10%), temperate conifer forest (59.66% ± 0.45%), and temperate evergreen forest (38.78 ± 0.49%) also show substantial area reductions relative to PVM estimates (Figure 4). These likely reflect widespread deforestation and land conversion, resulting in fragmented landscapes interspersed with grasslands, croplands, pastures, and urban areas (Ma et al., 2023). The use of finer-scale land cover products such as ESA-CCI improves the representation of sub-grid heterogeneity at 0.5° × 0.5° resolution, offering a more realistic alternative to the PVM's assumption of homogeneous vegetation.

3.6. Effects of N Fixation, Deposition, Weathering, and N_2O Uptake

To isolate the contributions of different nitrogen inputs to N_2O emissions, we conducted a sequential exclusion experiment, removing BNF, atmospheric deposition, and nitrogen weathering from the model. The decomposition analysis revealed that background emissions accounted for the largest portion (4.63 ± 0.15 Tg N yr^{-1}; 69.8 ± 4.5%), followed by nitrogen fixation (1.05 ± 0.15 Tg N yr^{-1}; 16.3% ± 2.6%), deposition (0.60 ± 0.04 Tg N yr^{-1}; 9.2% ± 1.3%), and weathering (0.30 ± 0.04 Tg N yr^{-1}; 4.7% ± 1.1%) (Figures 5a and 5b). These findings align with previous estimates, such as Cen et al. (2024), who reported that nitrogen deposition accounted for approximately 9.0% of global forest soil N_2O emissions. A similar pattern was observed for N_2O production, with background processes dominating (80.4% ± 2.9%) and smaller but non-negligible contributions from nitrogen fixation (9.3% ± 1.9%) and deposition (7.7 ± 1.6%).

While deposition and weathering remained stable, the contribution from nitrogen fixation rose significantly, from 13.7% (1990–1994) to 16.4% (2020–2023; $p < 0.001$, Sen's slope = +0.08% yr^{-1}). Conversely, N_2O uptake declined from 6.4% to 3.4% over the same period ($p < 0.001$, Sen's slope = −0.006% yr^{-1}), likely due to reduced atmospheric-soil concentration gradients as soil N_2O levels increased.

To evaluate the influence of land-cover representation on the attribution results, we conducted additional simulations using ESA-CCI based land-cover data and repeated the factor-contribution analysis. The decomposition analysis shows that background emissions account for the largest share (2.8 ± 0.06 Tg N yr^{-1}; 63.8 ± 0.9%), followed by BNF (1.03 ± 0.07 Tg N yr^{-1}; 23.3% ± 1.01%), atmospheric deposition (0.42 ± 0.01 Tg N yr^{-1}; 9.5% ± 0.35%), and rock weathering (0.15 ± 0.02 Tg N yr^{-1}; 3.38% ± 0.44%) (Figure S7 in Supporting Information S1). In comparison, the ESA-based simulations yielded lower contributions for background emissions but a higher relative contribution from BNF, although their rank order remained unchanged. Overall, while

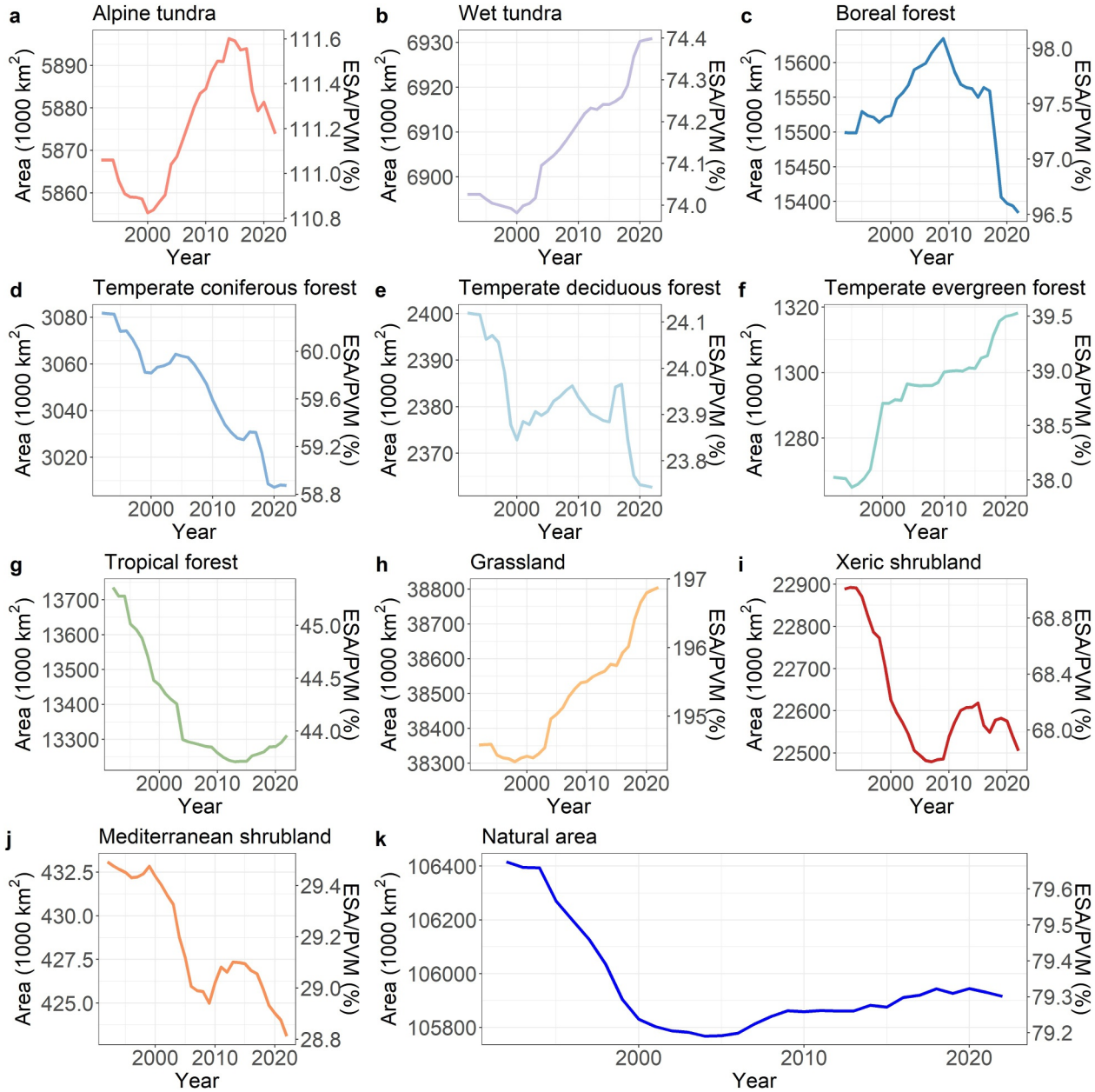

Figure 4. Temporal changes in ESA-derived plant functional type (PFT) areas from 1992 to 2022, based on European Space Agency Climate Change Initiative land cover data were converted to TEM-specific PFT classifications. Panels (a–j) show changes in the area and percentage of individual PFTs, while panel (k) displays the total natural area and the ratio of ESA-derived area to that from the potential vegetation map.

absolute magnitudes differ substantially between the two land-cover representations, primarily due to differences in the extent of natural land area, the relative ranking of drivers is consistent. This indicates that land-cover representation strongly affects total emission magnitude but exerts limited influence on the hierarchical importance of individual nitrogen inputs at the global scale. Consequently, the attribution of dominant controls on natural soil N_2O emissions remain robust across land-cover assumptions.

Several annual time-series nitrogen deposition data sets are available, including those from Ackerman et al. (2019) and Tian et al. (2022). To evaluate the potential impact of using linearly interpolated ACCMIP deposition data, we compared simulated N_2O emissions with an alternative simulation driven by the time-series HaNi deposition data set from Tian et al. (2022). The comparison shows that global natural soil N_2O emissions simulated with the HaNi data set are 0.15 ± 0.12 Tg N yr^{-1} ($2.3 \pm 1.8\%$) higher than those using the interpolated

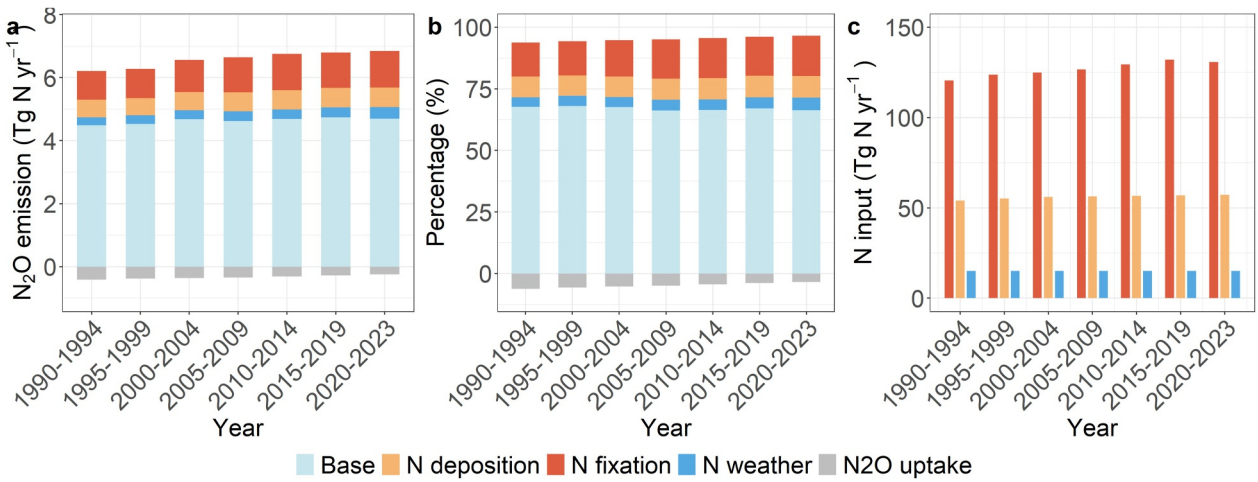

Figure 5. Panel (a) shows 5-year average simulated background N_2O emissions and contributions from biological nitrogen fixation, atmospheric nitrogen deposition, nitrogen weathering, and N_2O uptake based on the potential vegetation map. Panel (b) presents the corresponding percentage contributions of each component to total emissions. Panel (c) represents annual N inputs of nitrogen fixation, deposition and rock weathering (Tg N yr^{-1}).

ACCMIP data (Figure 6). Under the HaNi forcing, the simulated contributions from NOγ and NH_x deposition are 5.1 ± 0.76 Tg N yr^{-1} (19.2% ± 2.9%) and 12.43 ± 1.26 Tg N yr^{-1} (42.17% ± 3.6%) higher than those from ACCMIP, respectively.

This limited sensitivity arises because, at the global scale and in natural ecosystems, the interannual variability in nitrogen deposition is relatively small compared with its strong spatial gradients during the simulation period. As a result, the interpolation approach captures the dominant signal controlling long-term integrated N_2O emissions. This robustness also reflects the integrated long-term nature of soil nitrogen cycling, in which deposition represents second fraction of total nitrogen inputs, less than 10% compared with background emission and BNF. Consequently, differences in the temporal resolution of the deposition data sets have only a minor influence on the simulated global N_2O budget.

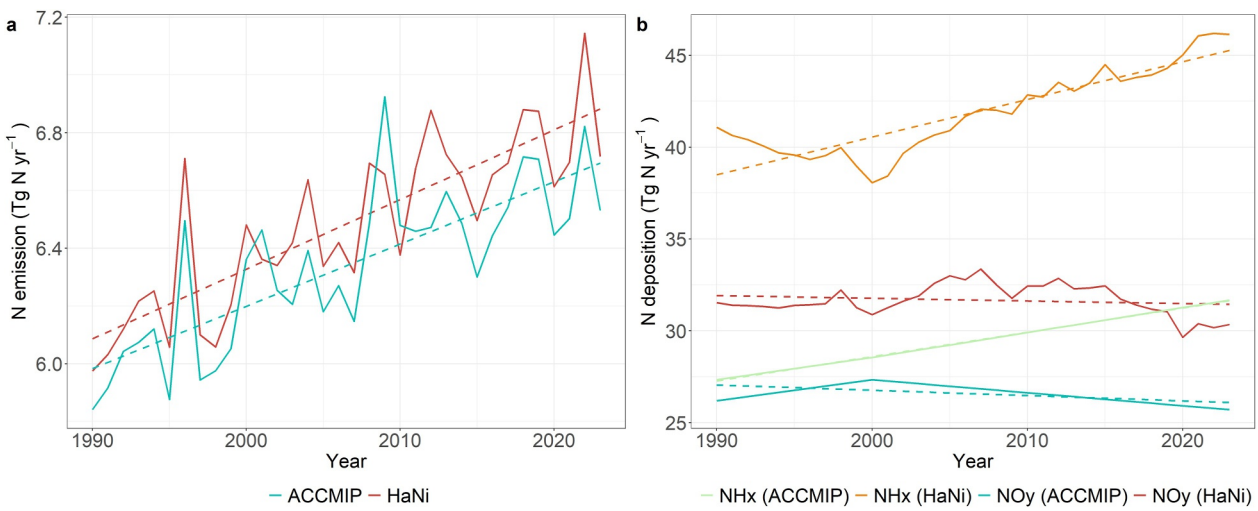

Figure 6. Temporal trends of global N_2O emissions simulated using the HaNi and ACCMIP nitrogen deposition data sets for the period 1990–2023 (a), and corresponding trends in NOγ and NH_x deposition from the two data sets (b).

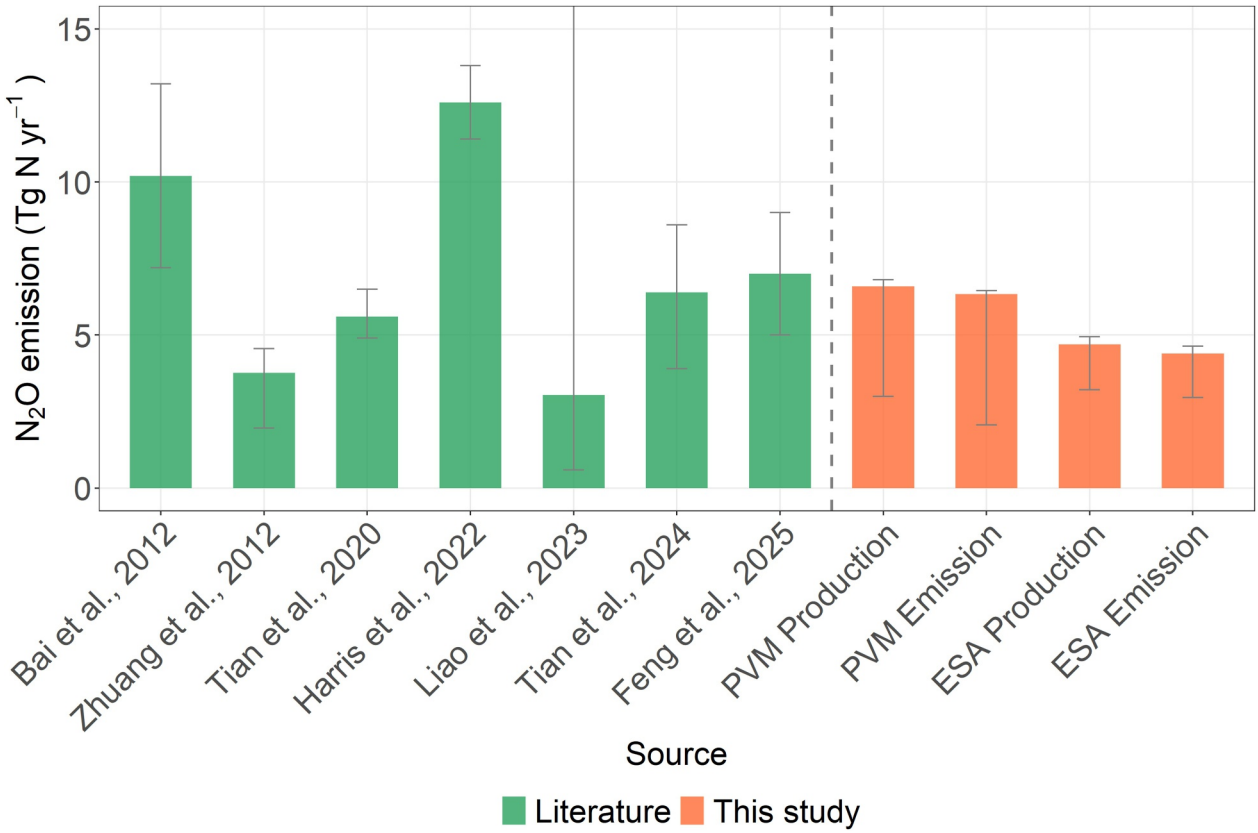

Figure 7. Comparison of annual N_2O emission estimates (Tg N yr^{-1}) from literature studies and model simulations. Error bars indicate reported uncertainty ranges.

4. Discussion

4.1. Comparison With Other Studies

Our model estimates are broadly consistent with recent literature when compared under comparable land-cover assumptions (Figure 7), although some discrepancies remain. Simulations using the ESA-CCI land cover yielded global N_2O production and emissions of 4.69 [3.21–4.95] and 4.40 [2.96–4.64] Tg N yr^{-1}, respectively. These values fall toward the lower end of previously reported ranges but remain within the overall uncertainty bounds of recent estimates based on contemporary land-use and land-cover conditions, including Tian et al. (2020, 2024; 5.6 [4.9–6.5] Tg N yr^{-1} and 6.4 [3.9–8.6] Tg N yr^{-1}), but lower than estimates from Feng et al. (2025; 7.0 ± 2.0 Tg N yr^{-1}), Bai et al. (2012; 10.2 ± 3.0 Tg N yr^{-1}), and Harris et al. (2022; 12.6 ± 1.2 Tg N yr^{-1}), and higher than the machine learning studies from Zhuang et al. (2012; 3.77 [1.96–4.56] Tg N yr^{-1}) and Liao et al. (2023; 3 [0.6–18.3] Tg N yr^{-1}). We calculated a global natural soil N_2O estimate by multiplying their reported mean emission rates by the global areas of forests and grasslands using a mean emission rate of 0.039 g N m^{-2} yr^{-1} for forests (range: 0.009–0.184 g N m^{-2} yr^{-1}) and 0.045 g N m^{-2} yr^{-1} for grasslands (range: 0.006–0.336 g N m^{-2} yr^{-1}). Using a global forest area of 4.14 billion hectares (FAO, 2025a) and a grassland area of 3.2 billion hectares (FAO, 2025b), this yields approximately 3 Tg N yr^{-1} (range: 0.6–18.3 Tg N yr^{-1}). The PVM-based simulations produced higher values (6.59 and 6.34 Tg N yr^{-1}), representing potential emissions under idealized natural vegetation. The difference between the ESA-CCI and PVM-based estimates highlights the strong sensitivity of modeled N_2O fluxes to land-cover representation. Recent studies generally report global natural soil N_2O emissions in the range of 4–9 Tg N yr^{-1} (e.g., Feng et al., 2025; Tian et al., 2020, 2024). Our ESA-CCI-based estimates fall toward the lower end of this range, while the PVM-based results are closer to the mid-to-upper portion. These differences largely reflect contrasting land-cover representations: the ESA-CCI based simulations account for historical land-use changes and exclude managed lands, whereas the PVM-based simulations represent potential natural vegetation under idealized conditions.

In addition, these discrepancies likely stem from differences in model parameterization, input data, and representation of key biogeochemical processes. Higher estimates from Bai et al. (2012) and Harris et al. (2022), which are based on isotope modeling, highlight methodological differences across approaches. The lower estimates reported by Zhuang et al. (2012) and Liao et al. (2023) may be attributed to differences in temporal coverage or that process-based models capture additional climate sensitivities not fully represented in the observationally trained machine learning models.

In our simulation, tropical regions contributed 70% of global N_2O emissions, consistent with the latitudinal gradient reported by Tian et al. (2019), which identified a single tropical peak accounting for 69% of global emissions. This pattern is also supported by the artificial neural network study by Zhuang et al. (2012). Our estimated tropical emission rate (0.114 ± 0.006 g N m^{-2} yr^{-1}) closely matches Tian et al.'s value (0.11 ± 0.02 g N m^{-2} yr^{-1}) but is approximately half the estimate reported by Feng et al. (2025; 0.21–0.28 g N m^{-2} yr^{-1}). For grasslands, our simulation yielded much lower N_2O emissions (0.035 ± 0.006 g N m^{-2} yr^{-1}) compared to Feng et al.'s range of 0.08–0.17 g N m^{-2} yr^{-1} across C_3 and C_4 grasses, about half the lower bound of their estimate. However, our estimate is closer to the value reported by Liao et al. (2023), which is 0.045 (0.006–0.336) g N m^{-2} yr^{-1} for grasslands.

4.2. Limitations and Future Directions

This study is subject to several limitations. First, model calibration and validation are restricted by the limited spatiotemporal coverage of observational data sets, particularly in dryland regions such as Africa and the Middle East (Figure S1 in Supporting Information S1). Expanding monitoring networks in these areas would improve the representation of key drivers, such as soil moisture, temperature, and nitrogen availability that regulate N_2O emissions. Increased use of isotopic techniques (e.g., $\delta^{15}N$) could also help distinguish microbial sources of N_2O, thereby enhancing our mechanistic understanding of the underlying processes. Strengthening the observational infrastructure would reduce model uncertainties and improve nitrogen cycle representation.

Second, the model's $0.5° \times 0.5°$ spatial resolution may not sufficiently capture the substantial heterogeneity in landscape features and soil properties such as soil organic carbon and total nitrogen stocks. While we used 300-m ESA-CCI land cover data for improved spatial detail, other inputs such as meteorology, soil, and topography remained uniform within each grid. Higher-resolution modeling could enhance N_2O estimates but at high computational cost. Therefore, developing innovative approaches to balance spatial resolution and computational efficiency is essential for future studies. Promising directions include knowledge-guided machine learning methods (Liu et al., 2022) and machine learning–based meta-models (Aderele et al., 2025), which can approximate complex biogeochemical processes at lower computational expense.

Third, using a monthly time step constrains the model's ability to capture short-term, high-impact events such as extreme precipitation, which are increasingly recognized as important drivers of elevated N_2O emissions due to their strong influence on soil moisture dynamics and microbial processes (Chen et al., 2025). Such events can disrupt hydrological regimes and biogeochemical cycles and boost greenhouse gas emissions (Hutchins et al., 2019; Vereecken et al., 2022). Moreover, reanalysis data sets such as ERA5 have demonstrated considerable errors in representing extreme precipitation, especially in tropical regions and China (Jiang et al., 2021; Lavers et al., 2022). These inaccuracies in meteorological inputs may further compound uncertainties in N_2O emission estimates, underscoring the need for bias-corrected climate forcing data sets in earth system modeling.

Fourth, our model does not account for perturbed fluxes resulting from land-cover change, which can cause significant time-varying shifts in N_2O emissions. The reduction in the calculated natural source is, however, accompanied by a large and well-documented increase in anthropogenic emissions from agricultural soils following land conversion. For instance, converting tropical forests to agriculture typically triggers a short-term emission pulse lasting up to 5 years, followed by a decline below those of the original forest, especially if pastures degrade or croplands are unfertilized (Davidson & Artaxo, 2004; Meurer et al., 2016). When abandoned farmland transitions to secondary forest, emissions rise slowly but usually stay below those of mature forests or fertilized fields (Davidson et al., 2007; Sullivan et al., 2019). Tian et al. (2024) modeled both the short-term increase in emissions from the post-deforestation pulse effect and the long-term decrease associated with the reduction of mature forest area. The combined effect of these transitions leads to a net reduction of approximately 0.5 Tg N_2O yr^{-1}, equivalent to 7.7% of total natural soil N_2O emissions. These dynamic effects remain unaccounted for in our framework and should be integrated into future modeling to better capture land-use impacts on N_2O fluxes.

5. Conclusion

This study identifies a persistent rise in global N_2O emissions from 1990 to 2023 (+0.021 Tg N yr^{-1}, $p < 0.001$), with tropical ecosystems accounting for 70% of the total flux. Emissions based on remote sensing land cover (ESA-CCI) were 30% lower than those using potential vegetation, highlighting how land use change, especially the reduction of tropical forests to 44.5% of their potential extent, leads to significant underestimation in global natural soil N_2O emissions. This quantification underscores that the contribution of natural ecosystems to the contemporary N_2O budget is declining not only due to changes in climate and N deposition but also due to their reduced physical extent. Accurately tracking this declining natural baseline is essential for attributing changes in the global budget to specific anthropogenic drivers (e.g., fertilizer use vs. land cover change).

Despite robust trends, uncertainties remain, stemming from limited observational data, simplifications in model structure, and biases in meteorological and land cover inputs. The coarse spatial and temporal resolution used in this study likely mask short-term pulse emissions linked to extreme weather events. Future modeling efforts would benefit higher-resolution simulations to better capture fine-scale variability and extreme event impacts. Addressing these limitations requires (a) higher-resolution modeling to capture fine-scale and event-driven variability and finer-resolution models to resolve short-term pulse emissions, (b) expanded use of isotopic techniques to attribute microbial pathways, and (c) integration of dynamic, time-varying land-use and land-cover changes into Earth system models.

Conflict of Interest

The authors declare no conflicts of interest relevant to this study.

Availability Statement

The TEM codes, outputs, and samples of the running directory can be accessed via the Purdue University Research Repository (Yuan & Zhuang, 2025).

Acknowledgments
This research has been supported by the National Science Foundation (Grant 1802832).

References

Ackerman, D., Millet, D. B., & Chen, X. (2019). Global estimates of inorganic nitrogen deposition across four decades. *Global Biogeochemical Cycles*, *33*(1), 100–107. https://doi.org/10.1029/2018gb005990

Aderele, M. O., Srivastava, A. K., Butterbach-Bahl, K., & Rahimi, J. (2025). Integrating machine learning with agroecosystem modelling: Current state and future challenges. *European Journal of Agronomy*, *168*, 127610. https://doi.org/10.1016/j.eja.2025.127610

Asaadi, A., & Arora, V. K. (2021). Implementation of nitrogen cycle in the CLASSIC land model. *Biogeosciences*, *18*(2), 669–706. https://doi.org/10.5194/bg-18-669-2021

Bai, E., Houlton, B. Z., & Wang, Y. P. (2012). Isotopic identification of nitrogen hotspots across natural terrestrial ecosystems. *Biogeosciences*, *9*(8), 3287–3304. https://doi.org/10.5194/bg-9-3287-2012

Butterbach-Bahl, K., Baggs, E. M., Dannenmann, M., Kiese, R., & Zechmeister-Boltenstern, S. (2013). Nitrous oxide emissions from soils: How well do we understand the processes and their controls? *Philosophical Transactions of the Royal Society B: Biological Sciences*, *368*(1621), 20130122. https://doi.org/10.1098/rstb.2013.0122

Carter, A. J., & Scholes, R. J. (2000). SoilData v2.0: Generating a global database of soil properties [Dataset]. *CSIR Environmentek, Pretoria, South Africa*. https://www.fao.org/soils-portal/data-hub/soil-maps-and-databases/harmonized-world-soil-database-v20/en/

Cen, X., Müller, C., Kang, X., Zhou, X., Zhang, J., Yu, G., & He, N. (2024). Nitrogen deposition contributed to a global increase in nitrous oxide emissions from forest soils. *Communications Earth & Environment*, *5*(1), 532. https://doi.org/10.1038/s43247-024-01647-6

Chen, Z., Zhang, N., Li, Y., Xu, S., Liu, Y., Miao, S., & Ding, W. (2025). Extreme rainfall amplified the stimulatory effects of soil carbon availability on N_2 O emissions. *Global Change Biology*, *31*(4), e70164. https://doi.org/10.1111/gcb.70164

Copernicus Climate Change Service, Climate Data Store. (2019). Land cover classification gridded maps from 1992 to present derived from satellite observation [Dataset]. *Copernicus Climate Change Service (C3S) Climate Data Store (CDS)*. https://doi.org/10.24381/cds.006f2c9a

Davidson, E. A., & Artaxo, P. (2004). Globally significant changes in biological processes of the Amazon Basin: Results of the large-scale Biosphere–Atmosphere experiment. *Global Change Biology*, *10*(5), 519–529. https://doi.org/10.1111/j.1529-8817.2003.00779.x

Davidson, E. A., De Carvalho, C. J. R., Figueira, A. M., Ishida, F. Y., Ometto, J. P. H. B., Nardoto, G. B., et al. (2007). Recuperation of nitrogen cycling in Amazonian forests following agricultural abandonment. *Nature*, *447*(7147), 995–998. https://doi.org/10.1038/nature05900

Davies-Barnard, T., Meyerholt, J., Zaehle, S., Friedlingstein, P., Brovkin, V., Fan, Y., et al. (2020). Nitrogen cycling in CMIP6 land surface models: Progress and limitations. *Biogeosciences*, *17*(20), 5129–5148. https://doi.org/10.5194/bg-17-5129-2020

Erb, K.-H., Kastner, T., Plutzar, C., Bais, A. L. S., Carvalhais, N., Fetzel, T., et al. (2018). Unexpectedly large impact of forest management and grazing on global vegetation biomass. *Nature*, *553*(7686), 73–76. https://doi.org/10.1038/nature25138

FAO. (2025a). Global forest resources assessment 2025: Main report. *Food and Agriculture Organization of the United Nations*. https://doi.org/10.4060/cd6709en

FAO. (2025b). Land statistics 2001–2023: Global, regional and country trends (FAOSTAT Analytical Briefs, No. 107). *Food and Agriculture Organization of the United Nations*. https://doi.org/10.4060/cd5765en

Feng, M., Liu, G., Wang, Y., Chang, J., & Peng, S. (2025). Isotopic partitioning of gaseous nitrogen emissions of natural terrestrial ecosystems. *Environmental Research Letters*, *20*(3), 034053. https://doi.org/10.1088/1748-9326/adbb06

Ghimire, B., Riley, W. J., Koven, C. D., Mu, M., & Randerson, J. T. (2016). Representing leaf and root physiological traits in CLM improves global carbon and nitrogen cycling predictions. *Journal of Advances in Modeling Earth Systems*, *8*(2), 598–613. https://doi.org/10.1002/2015MS000538

GLOBAL SOIL DATA TASK. (2000). Global gridded surfaces of selected soil characteristics (IGBP-DIS) [Dataset]. *ORNL Distributed Active Archive Center*. https://doi.org/10.3334/ORNLDAAC/569

Goll, D. S., Winkler, A. J., Raddatz, T., Dong, N., Prentice, I. C., Ciais, P., & Brovkin, V. (2017). Carbon–nitrogen interactions in idealized simulations with JSBACH (version 3.10). *Geoscientific Model Development*, *10*(5), 2009–2030. https://doi.org/10.5194/gmd-10-2009-2017

Harper, K. L., Lamarche, C., Hartley, A., Peylin, P., Ottlé, C., Bastrikov, V., et al. (2023). A 29-year time series of annual 300 m resolution plant-functional-type maps for climate models. *Earth System Science Data*, *15*(3), 1465–1499. https://doi.org/10.5194/essd-15-1465-2023

Harris, E., Yu, L., Wang, Y.-P., Mohn, J., Henne, S., Bai, E., et al. (2022). Warming and redistribution of nitrogen inputs drive an increase in terrestrial nitrous oxide emission factor. *Nature Communications*, *13*(1), 4310. https://doi.org/10.1038/s41467-022-32001-z

Hersbach, H., Bell, B., Berrisford, P., Biavati, G., Horányi, A., Muñoz Sabater, J., et al. (2023). ERA5 monthly averaged data on single levels from 1940 to present [Dataset]. *Copernicus Climate Change Service (C3S) Climate Data Store (CDS)*. https://doi.org/10.24381/cds.f17050d7

Houlton, B. Z., Morford, S. L., & Dahlgren, R. A. (2018). Convergent evidence for widespread rock nitrogen sources in Earth's surface environment. *Science*, *360*(6384), 58–62. https://doi.org/10.1126/science.aan4399

Hutchins, D. A., Jansson, J. K., Remais, J. V., Rich, V. I., Singh, B. K., & Trivedi, P. (2019). Climate change microbiology—Problems and perspectives. *Nature Reviews Microbiology*, *17*(6), 391–396. https://doi.org/10.1038/s41579-019-0178-5

Jiang, Q., Li, W., Fan, Z., He, X., Sun, W., Chen, S., et al. (2021). Evaluation of the ERA5 reanalysis precipitation dataset over Chinese Mainland. *Journal of Hydrology*, *595*, 125660. https://doi.org/10.1016/j.jhydrol.2020.125660

Kroeze, C., Mosier, A., & Bouwman, L. (1999). Closing the global N_2O budget: A retrospective analysis 1500–1994. *Global Biogeochemical Cycles*, *13*(1), 1–8. https://doi.org/10.1029/1998GB900020

Lamarque, J.-F., Dentener, F., McConnell, J., Ro, C.-U., Shaw, M., Vet, R., et al. (2013). Multi-model mean nitrogen and sulfur deposition from the Atmospheric Chemistry and Climate Model Intercomparison Project (ACCMIP): Evaluation of historical and projected future changes. *Atmospheric Chemistry and Physics*, *13*(16), 7997–8018. https://doi.org/10.5194/acp-13-7997-2013

Lavers, D. A., Simmons, A., Vamborg, F., & Rodwell, M. J. (2022). An evaluation of ERA5 precipitation for climate monitoring. *Quarterly Journal of the Royal Meteorological Society*, *148*(748), 3152–3165. https://doi.org/10.1002/qj.4351

Lawrence, D. M., Fisher, R. A., Koven, C. D., Oleson, K. W., Swenson, S. C., Bonan, G., et al. (2019). The community land model version 5: Description of new features, benchmarking, and impact of forcing uncertainty. *Journal of Advances in Modeling Earth Systems*, *11*(12), 4245–4287. https://doi.org/10.1029/2018MS001583

Liao, J., Huang, Y., Li, Z., & Niu, S. (2023). Data-driven modeling on the global annual soil nitrous oxide emissions: Spatial pattern and attributes. *Science of the Total Environment*, *903*, 166472. https://doi.org/10.1016/j.scitotenv.2023.166472

Liu, L., Xu, S., Tang, J., Guan, K., Griffis, T. J., Erickson, M. D., et al. (2022). KGML-ag: A modeling framework of knowledge-guided machine learning to simulate agroecosystems: A case study of estimating N_2 O emission using data from mesocosm experiments. *Geoscientific Model Development*, *15*(7), 2839–2858. https://doi.org/10.5194/gmd-15-2839-2022

Liu, S., Bond-Lamberty, B., Boysen, L. R., Ford, J. D., Fox, A., Gallo, K., et al. (2017). Grand challenges in understanding the interplay of climate and land changes. *Earth Interactions*, *21*(2), 1–43. https://doi.org/10.1175/EI-D-16-0012.1

Ma, J., Olin, S., Anthoni, P., Rabin, S. S., Bayer, A. D., Nyawira, S. S., & Arneth, A. (2022). Modeling symbiotic biological nitrogen fixation in grain legumes globally with LPJ-GUESS (v4.0, r10285). *Geoscientific Model Development*, *15*(2), 815–839. https://doi.org/10.5194/gmd-15-815-2022

Ma, L., Hurtt, G., Tang, H., Lamb, R., Lister, A., Chini, L., et al. (2023). Spatial heterogeneity of global forest aboveground carbon stocks and fluxes constrained by spaceborne LiDAR data and mechanistic modeling. *Global Change Biology*, *29*(12), 3378–3394. https://doi.org/10.1111/gcb.16682

Mathison, C., Burke, E., Hartley, A. J., Kelley, D. I., Burton, C., Robertson, E., et al. (2023). Description and evaluation of the JULES-ES set-up for ISIMIP2b. *Geoscientific Model Development*, *16*(14), 4249–4264. https://doi.org/10.5194/gmd-16-4249-2023

McGuire, A. D., Melillo, J. M., Kicklighter, D. W., Pan, Y., Xiao, X., Helfrich, J., et al. (1997). Equilibrium responses of global net primary production and carbon storage to doubled atmospheric carbon dioxide: Sensitivity to changes in vegetation nitrogen concentration. *Global Biogeochemical Cycles*, *11*(2), 173–189. https://doi.org/10.1029/97GB00059

Melillo, J. M., McGuire, A. D., Kicklighter, D. W., Moore, B., Vorosmarty, C. J., & Schloss, A. L. (1993). Global climate change and terrestrial net primary production. *Nature*, *363*(6426), 234–240. https://doi.org/10.1038/363234a0

Meurer, K. H. E., Franko, U., Stange, C. F., Rosa, J. D., Madari, B. E., & Jungkunst, H. F. (2016). Direct nitrous oxide (N_2 O) fluxes from soils under different land use in Brazil—A critical review. *Environmental Research Letters*, *11*(2), 023001. https://doi.org/10.1088/1748-9326/11/2/023001

Montes, F., Rotz, C. A., & Chaoui, H. (2009). Process modeling of ammonia volatilization from ammonium solution and manure surfaces: A review with recommended models. *Transactions of the ASABE*, *52*(5), 1707–1720. https://doi.org/10.13031/2013.29133

Morford, S. L., Houlton, B. Z., & Dahlgren, R. A. (2016). Direct quantification of long-term rock nitrogen inputs to temperate forest ecosystems. *Ecology*, *97*(1), 54–64. https://doi.org/10.1890/15-0501.1

NOAA Global Monitoring Laboratory. (2025). *Trends in atmospheric carbon dioxide*. National Oceanic and Atmospheric Administration. Retrieved from https://gml.noaa.gov/ccgg/trends/

Pielke, R. A. (2005). Land use and climate change. *Science*, *310*(5754), 1625–1626. https://doi.org/10.1126/science.1120529

Qu, Y., Maksyutov, S., & Zhuang, Q. (2018). Technical Note: An efficient method for accelerating the spin-up process for process-based biogeochemistry models. *Biogeosciences*, *15*(13), 3967–3973. https://doi.org/10.5194/bg-15-3967-2018

R Core Team. (2024). *R: A language and environment for statistical computing. Version 4.3.3*. R Foundation for Statistical Computing. Retrieved from https://www.R-project.org/

Stocker, B. D., Prentice, I. C., Cornell, S. E., Davies-Barnard, T., Finzi, A. C., Franklin, O., et al. (2016). Terrestrial nitrogen cycling in Earth system models revisited. *New Phytologist*, *210*(4), 1165–1168. https://doi.org/10.1111/nph.13997

Sullivan, B. W., Nifong, R. L., Nasto, M. K., Alvarez-Clare, S., Dencker, C. M., Soper, F. M., et al. (2019). Biogeochemical recuperation of lowland tropical forest during succession. *Ecology*, *100*(4), e02641. https://doi.org/10.1002/ecy.2641

Thompson, R. L., Lassaletta, L., Patra, P. K., Wilson, C., Wells, K. C., Gressent, A., et al. (2019). Acceleration of global N_2O emissions seen from two decades of atmospheric inversion. *Nature Climate Change*, *9*(12), 993–998. https://doi.org/10.1038/s41558-019-0613-7

Tian, H., Bian, Z., Shi, H., Qin, X., Pan, N., Lu, C., et al. (2022). History of anthropogenic Nitrogen inputs (HaNi) to the terrestrial biosphere: A 5 arcmin resolution annual dataset from 1860 to 2019. *Earth System Science Data*, *14*(10), 4551–4568. https://doi.org/10.5194/essd-14-4551-2022

Tian, H., Pan, N., Thompson, R. L., Canadell, J. G., Suntharalingam, P., Regnier, P., et al. (2024). Global nitrous oxide budget (1980–2020). *Earth System Science Data*, *16*(6), 2543–2604. https://doi.org/10.5194/essd-16-2543-2024

Tian, H., Xu, R., Canadell, J. G., Thompson, R. L., Winiwarter, W., Suntharalingam, P., et al. (2020). A comprehensive quantification of global nitrous oxide sources and sinks. *Nature*, *586*(7828), 248–256. https://doi.org/10.1038/s41586-020-2780-0

Tian, H., Yang, J., Xu, R., Lu, C., Canadell, J. G., Davidson, E. A., et al. (2019). Global soil nitrous oxide emissions since the preindustrial era estimated by an ensemble of terrestrial biosphere models: Magnitude, attribution, and uncertainty. *Global Change Biology*, *25*(2), 640–659. https://doi.org/10.1111/gcb.14514

Vereecken, H., Amelung, W., Bauke, S. L., Bogena, H., Brüggemann, N., Montzka, C., et al. (2022). Soil hydrology in the Earth system. *Nature Reviews Earth & Environment*, *3*(9), 573–587. https://doi.org/10.1038/s43017-022-00324-6

Vitousek, P. M., Menge, D. N. L., Reed, S. C., & Cleveland, C. C. (2013). Biological nitrogen fixation: Rates, patterns and ecological controls in terrestrial ecosystems. *Philosophical Transactions of the Royal Society B: Biological Sciences*, *368*(1621), 20130119. https://doi.org/10.1098/rstb.2013.0119

Vuichard, N., Messina, P., Luyssaert, S., Guenet, B., Zaehle, S., Ghattas, J., et al. (2019). Accounting for carbon and nitrogen interactions in the global terrestrial ecosystem model ORCHIDEE (trunk version, rev 4999): Multi-scale evaluation of gross primary production. *Geoscientific Model Development*, *12*(11), 4751–4779. https://doi.org/10.5194/gmd-12-4751-2019

Wan, J., Tokunaga, T. K., Brown, W., Newman, A. W., Dong, W., Bill, M., et al. (2021). Bedrock weathering contributes to subsurface reactive nitrogen and nitrous oxide emissions. *Nature Geoscience*, *14*(4), 217–224. https://doi.org/10.1038/s41561-021-00717-0

Wooliver, R., Pellegrini, A. F. A., Waring, B., Houlton, B. Z., Averill, C., Schimel, J., et al. (2019). Changing perspectives on terrestrial nitrogen cycling: The importance of weathering and evolved resource-use traits for understanding ecosystem responses to global change. *Functional Ecology*, *33*(10), 1818–1829. https://doi.org/10.1111/1365-2435.13377

Yuan, Y., & Zhuang, Q. (2025). Quantification of global terrestrial natural ecosystem nitrous oxide emissions from 1990 to 2023 with an improved nitrogen cycle modeling framework [Dataset]. https://doi.org/10.4231/G9QM-9V96

Yuan, Y., Zhuang, Q., Zhao, B., & Liu, L. (2025). Improving the quantification of global free-living and symbiotic nitrogen fixation in natural terrestrial ecosystems: Present-day estimates and 21st century projections. *Environmental Research Letters*, *20*(12), 124005. https://doi.org/10.1088/1748-9326/ae198c

Yuan, Y., Zhuang, Q., Zhao, B., & Shurpali, N. (2025). Impacts of permafrost degradation on N_2O emissions from natural terrestrial ecosystems in northern high latitudes: A process-based biogeochemistry model analysis. *Global Biogeochemical Cycles*, *39*(4), e2024GB008439. https://doi.org/10.1029/2024GB008439

Zhao, B., & Zhuang, Q. (2024). Nitrogen cycling feedback on carbon dynamics leads to greater CH_4 emissions and weaker cooling effect of Northern peatlands. *Global Biogeochemical Cycles*, *38*(4), e2023GB007978. https://doi.org/10.1029/2023GB007978

Zhu, Q., Riley, W. J., Tang, J., Collier, N., Hoffman, F. M., Yang, X., & Bisht, G. (2019). Representing nitrogen, phosphorus, and carbon interactions in the E3SM land model: Development and global benchmarking. *Journal of Advances in Modeling Earth Systems*, *11*(7), 2238–2258. https://doi.org/10.1029/2018MS001571

Zhuang, Q., Lu, Y., & Chen, M. (2012). An inventory of global N_2O emissions from the soils of natural terrestrial ecosystems. *Atmospheric Environment*, *47*, 66–75. https://doi.org/10.1016/j.atmosenv.2011.11.036

Zhuang, Q., McGuire, A. D., Melillo, J. M., Clein, J. S., Dargaville, R. J., Kicklighter, D. W., et al. (2003). Carbon cycling in extratropical terrestrial ecosystems of the Northern Hemisphere during the 20th century: A modeling analysis of the influences of soil thermal dynamics. *Tellus B: Chemical and Physical Meteorology*, *55*(3), 751–776. https://doi.org/10.1034/j.1600-0889.2003.00060.x

Zhuang, Q., McGuire, A. D., O'Neill, K. P., Harden, J. W., Romanovsky, V. E., & Yarie, J. (2002). Modeling soil thermal and carbon dynamics of a fire chronosequence in interior Alaska. *Journal of Geophysical Research*, *107*(D1). https://doi.org/10.1029/2001JD001244

References From the Supporting Information

Aini, F. K., Hergoualc'h, K., Smith, J. U., & Verchot, L. (2015). Nitrous oxide emissions along a gradient of tropical forest disturbance on mineral soils in Sumatra. *Agriculture, Ecosystems & Environment*, *214*, 107–117. https://doi.org/10.1016/j.agee.2015.08.022

Alvarez, C. R., Rimski-Korsakov, H., Lupi, A. M., Romaniuk, R. I., Cosentino, V. R. N., Ciarlo, E. A., & Steinbach, H. S. (2020). Soil nitrous oxide emissions from Eucalyptus plantation in Argentina. *Forest Ecology and Management*, *473*, 118301. https://doi.org/10.1016/j.foreco.2020.118301

Bell, M. J., Cloy, J. M., Topp, C. F. E., Ball, B. C., Bagnall, A., Rees, R. M., & Chadwick, D. R. (2016). Quantifying N_2O emissions from intensive grassland production: The role of synthetic fertilizer type, application rate, timing and nitrification inhibitors. *The Journal of Agricultural Science*, *154*(5), 812–827. https://doi.org/10.1017/S0021859615000945

Bowden, R. D., Rullo, G., Stevens, G. R., & Steudler, P. A. (2000). Soil fluxes of carbon dioxide, nitrous oxide, and methane at a productive temperate deciduous Forest. *Journal of Environmental Quality*, *29*(1), 268–276. https://doi.org/10.2134/jeq2000.00472425002900010034x

Butterbach-Bahl, K., Gasche, R., Huber, C., Kreutzer, K., & Papen, H. (1998). Impact of N-input by wet deposition on N-trace gas fluxes and CH4-oxidation in spruce forest ecosystems of the temperate zone in Europe. *Atmospheric Environment*, *32*(3), 559–564. https://doi.org/10.1016/S1352-2310(97)00234-3

Cantarel, A. A. M., Bloor, J. M. G., Deltroy, N., & Soussana, J.-F. (2011). Effects of climate change drivers on nitrous oxide fluxes in an upland temperate grassland. *Ecosystems*, *14*(2), 223–233. https://doi.org/10.1007/s10021-010-9405-7

Chen, H., Gurmesa, G. A., Zhang, W., Zhu, X., Zheng, M., Mao, Q., et al. (2016). Nitrogen saturation in humid tropical forests after 6 years of nitrogen and phosphorus addition: Hypothesis testing. *Functional Ecology*, *30*(2), 305–313. https://doi.org/10.1111/1365-2435.12475

Christiansen, J. R., Gundersen, P., Frederiksen, P., & Vesterdal, L. (2012). Influence of hydromorphic soil conditions on greenhouse gas emissions and soil carbon stocks in a Danish temperate forest. *Forest Ecology and Management*, *284*, 185–195. https://doi.org/10.1016/j.foreco.2012.07.048

Cui, Q., Song, C., Wang, X., Shi, F., Yu, X., & Tan, W. (2018). Effects of warming on N_2O fluxes in a boreal peatland of Permafrost region, Northeast China. *Science of the Total Environment*, *616–617*, 427–434. https://doi.org/10.1016/j.scitotenv.2017.10.246

Dannenmann, M., Díaz-Pinés, E., Kitzler, B., Karhu, K., Tejedor, J., Ambus, P., et al. (2018). Postfire nitrogen balance of Mediterranean shrublands: Direct combustion losses versus gaseous and leaching losses from the postfire soil mineral nitrogen flush. *Global Change Biology*, *24*(10), 4505–4520. https://doi.org/10.1111/gcb.14388

Davidson, E. A., Nepstad, D. C., Ishida, F. Y., & Brando, P. M. (2008). Effects of an experimental drought and recovery on soil emissions of carbon dioxide, methane, nitrous oxide, and nitric oxide in a moist tropical forest. *Global Change Biology*, *14*(11), 2582–2590. https://doi.org/10.1111/j.1365-2486.2008.01694.x

Drewer, J., Lohila, A., Aurela, M., Laurila, T., Minkkinen, K., Penttilä, T., et al. (2010). Comparison of greenhouse gas fluxes and nitrogen budgets from an ombotrophic bog in Scotland and a minerotrophic sedge fen in Finland. *European Journal of Soil Science*, *61*(5), 640–650. https://doi.org/10.1111/j.1365-2389.2010.01267.x

Fan, S., & Yoh, M. (2020). Nitrous oxide emissions in proportion to nitrification in moist temperate forests. *Biogeochemistry*, *148*(3), 223–236. https://doi.org/10.1007/s10533-02000655-w

Fierro, A., & Castaldi, S. (2011). Soil N_2O emissions in a Mediterranean shrubland disturbed by experimental fires. *International Journal of Wildland Fire*, *20*(7), 847–855. https://doi.org/10.1071/WF10120

Glatzel, S., & Stahr, K. (2001). Methane and nitrous oxide exchange in differently fertilised grassland in southern Germany. *Plant and Soil*, *231*(1), 21–35. https://doi.org/10.1023/A:1010315416866

Goldberg, S. D., & Gebauer, G. (2009). N_2O and NO fluxes between a Norway spruce forest soil and atmosphere as affected by prolonged summer drought. *Soil Biology and Biochemistry*, *41*(9), 1986–1995. https://doi.org/10.1016/j.soilbio.2009.07.001

Gong, Y., Wu, J., Vogt, J., & Le, T. B. (2019). Warming reduces the increase in N_2O emission under nitrogen fertilization in a boreal peatland. *Science of the Total Environment*, *664*, 72–78. https://doi.org/10.1016/j.scitotenv.2019.02.012

Guilbault, M. R., & Matthias, A. D. (1998). Emissions of N_2O from Sonoran Desert and effluent-irrigated grass ecosystems. *Journal of Arid Environments*, *38*(1), 87–98. https://doi.org/10.1006/jare.1997.0300

Guo, Y., Dong, Y., Peng, Q., Li, Z., He, Y., Yan, Z., & Qin, S. (2022). Effects of nitrogen and water addition on N2O emissions in temperate grasslands, northern China. *Applied Soil Ecology*, *177*, 104548. https://doi.org/10.1016/j.apsoil.2022.104548

Heinzle, J., Kitzler, B., Zechmeister-Boltenstern, S., Tian, Y., Kwatcho Kengdo, S., Wanek, W., et al. (2023). Soil CH_4 and N_2O response diminishes during decadal soil warming in a temperate mountain forest. *Agricultural and Forest Meteorology*, *329*, 109287. https://doi.org/10.1016/j.agrformet.2022.109287

Jiang, C., Yu, G., Fang, H., Cao, G., & Li, Y. (2010). Short-term effect of increasing nitrogen deposition on CO_2, CH_4 and N_2O fluxes in an alpine meadow on the Qinghai-Tibetan Plateau, China. *Atmospheric Environment*, *44*(24), 2920–2926. https://doi.org/10.1016/j.atmosenv.2010.03.030

Jones, S. K., Rees, R. M., Skiba, U. M., & Ball, B. C. (2005). Greenhouse gas emissions from a managed grassland. *Global and Planetary Change*, *47*(2–4), 201–211. https://doi.org/10.1016/j.gloplacha.2004.10.011

Jørgensen, C. J., & Elberling, B. (2012). Effects of flooding-induced N2O production, consumption and emission dynamics on the annual N2O emission budget in wetland soil. *Soil Biology and Biochemistry*, *53*, 9–17. https://doi.org/10.1016/j.soilbio.2012.05.005

Kiese, R., Hewett, B., Graham, A., & Butterbach-Bahl, K. (2003). Seasonal variability of N2 O emissions and CH4 uptake by tropical rainforest soils of Queensland, Australia. *Global Biogeochemical Cycles*, *17*(2), 2002GB002014. https://doi.org/10.1029/2002GB002014

Kim, Y. S. (2013). Soil-atmosphere exchange of CO_2, CH_4 and N_2O in northern temperate forests: Effects of elevated CO_2 concentration, N deposition and forest fire. *Eurasian journal of forest research*, *16*(1), 1–43.

Lafuente, A., Recio, J., Ochoa-Hueso, R., Gallardo, A., Pérez-Corona, M. E., Manrique, E., & Durán, J. (2020). Simulated nitrogen deposition influences soil greenhouse gas fluxes in a Mediterranean dryland. *Science of the Total Environment*, *737*, 139610. https://doi.org/10.1016/j.scitotenv.2020.139610

Li, K., Gong, Y., Song, W., Lv, J., Chang, Y., Hu, Y., et al. (2012). No significant nitrous oxide emissions during spring thaw under grazing and nitrogen addition in an alpine grassland. *Global Change Biology*, *18*(8), 2546–2554. https://doi.org/10.1111/j.1365-2486.2012.02704.x

Liu, X., Zhang, Q., Li, S., Zhang, L., & Ren, J. (2017). Simulated NH_4 + -N Deposition Inhibits CH_4 Uptake and promotes N_2O emission in the Meadow Steppe of Inner Mongolia, China. *Pedosphere*, *27*(2), 306–317. https://doi.org/10.1016/S1002-0160(17)60318-7

Lohila, A., Aurela, M., Hatakka, J., Pihlatie, M., Minkkinen, K., Penttilä, T., & Laurila, T. (2010). Responses of N_2O fluxes to temperature, water table and N deposition in a northern boreal fen. *European Journal of Soil Science*, *61*(5), 651–661. https://doi.org/10.1111/j.13652389.2010.01265.x

Maljanen, M., Alm, J., Martikainen, P. J., & Repo, T. (2010). Prolongation of soil frost resulting from reduced snow cover increases nitrous oxide emissions from boreal forest soil.

Maljanen, M., Jokinen, H., Saari, A., Strömmer, R., & Martikainen, P. J. (2006). Methane and nitrous oxide fluxes, and carbon dioxide production in boreal forest soil fertilized with wood ash and nitrogen. *Soil Use & Management*, *22*(2), 151–157. https://doi.org/10.1111/j.14752743.2006.00029.x

Matson, A., Pennock, D., & Bedard-Haughn, A. (2009). Methane and nitrous oxide emissions from mature forest stands in the boreal forest, Saskatchewan, Canada. *Forest Ecology and Management*, *258*(7), 1073–1083. https://doi.org/10.1016/j.foreco.2009.05.034

McCalley, C. K., Strahm, B. D., Sparks, K. L., Eller, A. S. D., & Sparks, J. P. (2011). The effect of long-term exposure to elevated CO_2 on nitrogen gas emissions from Mojave Desert soils. *Journal of Geophysical Research*, *116*(G3), G03022. https://doi.org/10.1029/2011JG001667

Merbold, L., Steinlin, C., & Hagedorn, F. (2013). Winter greenhouse gas fluxes (CO_2, CH_4 N_2O) from a subalpine grassland. *Biogeosciences*, *10*(5), 3185–3203. https://doi.org/10.5194/bg-103185-2013

Morishita, T., Aizawa, S., Yoshinaga, S., & Kaneko, S. (2011). Seasonal change in N2 O flux from forest soils in a forest catchment in Japan. *Journal of Forest Research*, *16*(5), 386–393. https://doi.org/10.1007/s10310-011-0285-2

Morishita, T., Matsuura, Y., Kajimoto, T., Osawa, A., Zyryanova, O. A., & Prokushkin, A. S. (2014). CH4 and N2O dynamics of a Larix gmelinii forest in a continuous permafrost region of central Siberia during the growing season. *Polar Science*, *8*(2), 156–165. https://doi.org/10.1016/j.polar.2014.01.004

Pang, J., Peng, C., Wang, X., Zhang, H., & Zhang, S. (2023). Soil-atmosphere exchange of carbon dioxide, methane and nitrous oxide in temperate forests along an elevation gradient in the Qinling Mountains, China. *Plant and Soil*, *488*(1–2), 325–342. https://doi.org/10.1007/s11104023-05967-y

Peichl, M., Arain, M. A., Ullah, S., & Moore, T. R. (2010). Carbon dioxide, methane, and nitrous oxide exchanges in an age-sequence of temperate pine forests. *Global Change Biology*, *16*(8), 2198–2212. https://doi.org/10.1111/j.1365-2486.2009.02066.x

Phillips, R. L., Whalen, S. C., & Schlesinger, W. H. (2001). Influence of atmospheric CO2 enrichment on nitrous oxide flux in a temperate forest ecosystem. *Global Biogeochemical Cycles*, *15*(3), 741–752. https://doi.org/10.1029/2000GB001372

Rowlings, D. W., Grace, P. R., Kiese, R., & Weier, K. L. (2012). Environmental factors controlling temporal and spatial variability in the soil-atmosphere exchange of CO2, CH4 and N2 O from an Australian subtropical rainforest. *Global Change Biology*, *18*(2), 726–738. https://doi.org/10.1111/j.1365-2486.2011.02563.x

Shvaleva, A., Lobo-do-Vale, R., Cruz, C., Castaldi, S., Rosa, A. P., Chaves, M. M., & Pereira, J. S. (2011). Soil-atmosphere greenhouse gases (CO2, CH4 and N2O) exchange in evergreen oak woodland in southern Portugal. *Plant Soil and Environment*, *57*(10), 471–477. https://doi.org/10.17221/223/2011-PSE

Soper, F. M., Sullivan, B. W., Nasto, M. K., Osborne, B. B., Bru, D., Balzotti, C. S., et al. (2018). Remotely sensed canopy nitrogen correlates with nitrous oxide emissions in a lowland tropical rainforest. *Ecology*, *99*(9), 2080–2089. https://doi.org/10.1002/ecy.2434

Sousa Neto, E., Carmo, J. B., Keller, M., Martins, S. C., Alves, L. F., Vieira, S. A., et al. (2011). Soil-atmosphere exchange of nitrous oxide, methane and carbon dioxide in a gradient of elevation in the coastal Brazilian Atlantic forest. *Biogeosciences*, *8*(3), 733–742. https://doi.org/10.5194/bg-8-733-2011

Stuart Grandy, A., & Philip Robertson, G. (2006). Initial cultivation of a temperate-region soil immediately accelerates aggregate turnover and CO2 and N2 O fluxes. *Global Change Biology*, *12*(8), 1507–1520. https://doi.org/10.1111/j.1365-2486.2006.01166.x

Takakai, F., Desyatkin, A. R., Lopez, C. M. L., Fedorov, A. N., Desyatkin, R. V., & Hatano, R. (2008). CH_4 and N_2O emissions from a forest-alas ecosystem in the permafrost taiga forest region, eastern Siberia, Russia. *Journal of Geophysical Research*, *113*(G2), 2007JG000521. https://doi.org/10.1029/2007JG000521

Ullah, S., & Moore, T. R. (2011). Biogeochemical controls on methane, nitrous oxide, and carbon dioxide fluxes from deciduous forest soils in eastern Canada. *Journal of Geophysical Research*, *116*(G3), G03010. https://doi.org/10.1029/2010JG001525

Vanitchung, S., Conrad, R., Harvey, N. W., & Chidthaisong, A. (2011). Fluxes and production pathways of nitrous oxide in different types of tropical forest soils in Thailand. *Soil Science & Plant Nutrition*, *57*(5), 650–658. https://doi.org/10.1080/00380768.2011.608168

Voigt, C., Lamprecht, R. E., Marushchak, M. E., Lind, S. E., Novakovskiy, A., Aurela, M., et al. (2017). Warming of subarctic tundra increases emissions of all three important greenhouse gases - Carbon dioxide, methane, and nitrous oxide. *Global Change Biology*, *23*(8), 3121–3138. https://doi.org/10.1111/gcb.13563

Wang, F., Li, J., Wang, X., Zhang, W., Zou, B., Neher, D. A., & Li, Z. (2014). Nitrogen and phosphorus addition impact soil N_2O emission in a secondary tropical forest of South China. *Scientific Reports*, *4*(1), 5615. https://doi.org/10.1038/srep05615

Wen, Y., Corre, M. D., Rachow, C., Chen, L., & Veldkamp, E. (2017). Nitrous oxide emissions from stems of alder, beech and spruce in a temperate forest. *Plant and Soil*, *420*(1–2), 423–434. https://doi.org/10.1007/s11104-017-3416-5

Wu, X., Brüggemann, N., Gasche, R., Shen, Z., Wolf, B., & Butterbach-Bahl, K. (2010). Environmental controls over soil-atmosphere exchange of N_2O, NO, and CO_2 in a temperate Norway spruce forest: Spruce forest N_2O, NO, and CO_2 soil fluxes. *Global Biogeochemical Cycles*, *24*(2). https://doi.org/10.1029/2009GB003616

Wu, X., Zang, S., Ma, D., Ren, J., Chen, Q., & Dong, X. (2019). Emissions of CO2, CH4, and N2O fluxes from Forest soil in Permafrost Region of Daxing'an Mountains, Northeast China. *International Journal of Environmental Research and Public Health*, *16*(16), 2999. https://doi.org/10.3390/ijerph16162999

Xu, K., Wang, C., & Yang, X. (2018). Five-year study of the effects of simulated nitrogen deposition levels and forms on soil nitrous oxide emissions from a temperate forest in northern China. *PLoS One*, *13*(4), e0196622. https://doi.org/10.1371/journal.pone.0196622

Xu, W., Frendrup, L. L., Michelsen, A., Elberling, B., & Ambus, P. L. (2023). Deepened snow in combination with summer warming increases growing season nitrous oxide emissions in dry tundra, but not in wet tundra. *Soil Biology and Biochemistry*, *180*, 109013. https://doi.org/10.1016/j.soilbio.2023.109013

Yan, Y., Ganjurjav, H., Hu, G., Liang, Y., Li, Y., He, S., et al. (2018). Nitrogen deposition induced significant increase of N2O emissions in an dry alpine meadow on the central Qinghai Tibetan Plateau. *Agriculture, Ecosystems & Environment*, *265*, 45–53. https://doi.org/10.1016/j.agee.2018.05.031

Yan, Y., Sha, L., Cao, M., Zheng, Z., Tang, J., Wang, Y., et al. (2008). Fluxes of CH4 and N2O from soil under a tropical seasonal rain forest in Xishuangbanna, Southwest China. *Journal of Environmental Sciences*, *20*(2), 207–215. https://doi.org/10.1016/S1001-0742(08)60033-9

Yue, P., Li, K., Hu, Y., Qiao, J., Wang, S., Ma, X., et al. (2024). The effect of nitrogen input on N2O emission depends on precipitation in a temperate desert steppe. *Science of the Total Environment*, *924*, 171572. https://doi.org/10.1016/j.scitotenv.2024.171572

Yue, P., Zuo, X., Li, K., Cui, X., Wang, S., Misselbrook, T., & Liu, X. (2021). The driving effect of nitrogen-related functional microorganisms under water and nitrogen addition on N2O emission in a temperate desert. *Science of the Total Environment*, *772*, 145470. https://doi.org/10.1016/j.scitotenv.2021.145470

Zhang, J., & Han, X. (2008). N2O emission from the semi-arid ecosystem under mineral fertilizer (urea and superphosphate) and increased precipitation in northern China. *Atmospheric Environment*, *42*(2), 291–302. https://doi.org/10.1016/j.atmosenv.2007.09.036

Zhang, W., Mo, J., Yu, G., Fang, Y., Li, D., Lu, X., & Wang, H. (2008). Emissions of nitrous oxide from three tropical forests in Southern China in response to simulated nitrogen deposition. *Plant and Soil*, *306*(1–2), 221–236. https://doi.org/10.1007/s11104-008-9575-7